

Mitigating controller noise in quantum gates using optimal control theory

Aviv Aroch* and Ronnie Kosloff

The Institute of Chemistry, The Hebrew University of Jerusalem, Jerusalem 9190401, Israel

Shimshon Kallush

Sciences Department, Holon Academic Institute of Technology,

52 Golomb Street, Holon 58102, Israel

All quantum systems are subject to noise from the environment or external controls. This noise is a major obstacle to the realization of quantum technology. For example, noise limits the fidelity of quantum gates. Employing optimal control theory, we study the generation of quantum single and two-qubit gates. Specifically, we explore a Markovian model of phase and amplitude noise, leading to the degradation of the gate fidelity. We show that optimal control with such noise models generates control solutions to mitigate the loss of gate fidelity. The problem is formulated in Liouville space employing an extremely accurate numerical solver and the Krotov algorithm for solving the optimal control equations.

I. INTRODUCTION

In reality, any quantum system is open. External intervention transforms the unitary dynamics of a closed system into a non-unitary evolution of an open one. We can classify three significant sources of such intervention: I. A thermal environment. II. Back-action due to quantum measurement. III. Noise originating from the external controller. This associated loss of coherence is the main obstacle in achieving quantum technology [1, 2]. The aim of this study is to explore the use of optimal control theory to mitigate the fidelity destruction of a quantum gate due to controller noise.

We formulate the dynamics of open quantum systems by considering completely positive trace-preserving maps (CPTP) [3]. In the Markovian limit, CPTP maps are generated by

* aviv.aroch@mail.huji.ac.il

the equation:

$$\frac{\partial}{\partial t} \hat{\rho} = \mathcal{L} \hat{\rho}$$

Where the generator \mathcal{L} has the Gorini, Kossakowski, Lindblad, Sudarshan (GKLS) structure [4, 5]. We adopt this framework for the present study.

Optimal control theory (OCT) has addressed open-system control problems [6–14]. In this case the generator of the dynamics \mathcal{L} becomes explicitly time-dependent a function of the control field $\mathcal{L}(\epsilon(t))$. This observation raises the issue: Are the dissipative and unitary dynamics linked? Does a change in the control field modify the dissipative dynamics? Consistency with thermodynamics imposes additional restrictions on the form of the master equation of a thermal environment [15]. In this case, the dissipative and the unitary parts are linked. Employing a thermodynamically consistent master equation, optimal control of quantum state-to-state and quantum gates was studied [16]. It was demonstrated that both entropy-changing and preserving transformations can be achieved. In particular, the negative aspect of dissipation on the fidelity of quantum gates could be mitigated. The mechanism identified can be described as active refrigeration accompanying the control process leading to a unitary quantum gate. A common approach to mitigating environmental noise is dynamical decoupling [11, 17]. Nevertheless, this method is not immune to noise on the controller.

In the present study, we deal with a different dissipative mechanism noise originating from the controller. This immediately imposes a link between the dissipative and unitary dynamics. Previous studies have shown that such noise leads to loss of purity and is therefore harmful to quantum control [18, 19]. Specifically, we address quantum systems with amplitude and phase noise, [20].

Our primary concern is exploring quantum control strategies to mitigate noise and maintain high-fidelity gates. We address this issue by employing optimal control theory first to generate unitary quantum gates in a pure Hamiltonian setup. We study both single and two-qubit gates forming a universal computation set. High-fidelity unitary gates are obtained. We now add noise to the controller and observe the degradation of fidelity. On this reference gate, we apply open system control, including noise, to mitigate the influence of this noise as much as possible. The paper is arranged as follows: Section II describes the noise model and the optimal control equations. Section III describes the results, which are discussed and summarized in the concluding Sec. IV.

II. QUANTUM NOISY DYNAMICS

The noisy dynamics are modeled within open quantum systems [21]. Expressly, we assume a quantum dynamical semi-group describes Markovian dynamics. The generator of such dynamics has the form of Gorini, Kossakowski, Lindblad, and Sudarshan master equation (GKLS) [5, 22]:

$$\frac{d}{dt}\hat{\rho}(t) = \mathcal{L}\hat{\rho} = -\frac{i}{\hbar}[\hat{\mathbf{H}}, \hat{\rho}] + \mathcal{D}\hat{\rho} \quad (1)$$

$\hat{\mathbf{H}}$ is the systems Hamiltonian, \mathcal{D} is the dissipative generator. \mathcal{L} , and \mathcal{D} are termed super-operators as they map operators in Hilbert space to other operators.

A. Noise model

We consider a quantum system controlled by an external field. The Hamiltonian of the system:

$$\hat{\mathbf{H}} = \hat{\mathbf{H}}_0 + \varepsilon(t)\hat{\mathbf{H}}_c \quad (2)$$

where $\hat{\mathbf{H}}_0$ is the drift Hamiltonian and $\hat{\mathbf{H}}_c$ is the control Hamiltonian and $\varepsilon(t)$ describes the time dependent control field. We aim to study the influence of noise originating from the controller (The pulse generator). We differentiate between two models of control noise: amplitude and phase noise. For amplitude noise, we consider random fluctuations in the amplitude of the control field $\varepsilon(t) = \varepsilon_c(t) + \xi(t)$. Assuming the controller is fast relative to the system dynamics We chose to model the noise as a Gaussian random process $\langle \xi(t)\xi(t') \rangle = \sqrt{2\gamma}\delta(t - t')$. Under these conditions, the dissipative part of Eq. (1) is generated from $\hat{\mathbf{H}}_c$ [4, 23, 24]:

$$\mathcal{D}_A = -\gamma_A \varepsilon_c^2(t) [\hat{\mathbf{H}}_c, [\hat{\mathbf{H}}_c, \bullet]] \quad (3)$$

where γ is the noise strength. Phase noise originates from timing errors in the controller [25, 26] or fluctuations in frequency [27]. Assuming a Gaussian white noise model, the dephasing generator becomes [25]:

$$\mathcal{D}_P = -\gamma_P [\hat{\mathbf{H}}, [\hat{\mathbf{H}}, \bullet]] \quad (4)$$

In both cases, the dissipator depends on the control field.

B. Vectorizing Liouville space

We describe the dynamics employing the Hilbert space of system operators defined by the scalar product. $(\hat{\mathbf{A}} \cdot \hat{\mathbf{B}}) = \text{tr}\{\hat{\mathbf{A}}^\dagger \hat{\mathbf{B}}\}$. Superoperators map operators into the same Hilbert space. We, therefore, choose to describe operators as vectors and superoperators by matrix-vector multiplications. We can now decompose a general operator $\hat{\mathbf{X}}$ employing a full orthogonal operator basis,

$$\{\hat{\mathbf{A}}\} = [\hat{\mathbf{A}}_1, \hat{\mathbf{A}}_2, \dots, \hat{\mathbf{A}}_N] \quad , \quad \text{tr}\{\hat{\mathbf{A}}_i^\dagger \cdot \hat{\mathbf{A}}_j\} = \delta_{ij}$$

Using this basis, we can represent $\hat{\mathbf{X}}$ as;

$$\hat{\mathbf{X}} = \sum_i \chi_i \hat{\mathbf{A}}_i \quad (5)$$

where χ_i is an element of a vector \vec{x} of expansion coefficients of size N^2 that characterizes $\hat{\mathbf{X}}$. Using this notation, we can define any operator of the dimension $N \times N$ with a vector of size N^2 .

In this formalism the mapping of a super-operator $\Lambda \hat{\mathbf{X}} = \hat{\mathbf{Y}}$ translates to a matrix-vector multiplication: $\tilde{\mathcal{G}}\vec{\chi} = \vec{v}$ where $\hat{\mathbf{Y}} = \sum_i v_i \hat{\mathbf{A}}_i$. The dynamical equation Eq. (1) can be reduced to a series of matrix-vector multiplications where $\vec{\rho}$ will denote to $\hat{\rho}$ in vector space, and $\tilde{\mathcal{L}}$ will denote the superoperator \mathcal{L} . For Additional details, Cf. ref. [28]. (Throughout this paper, we will use the notation " \sim " to assign a super operator in Liouville space). The action of the superoperator on the density operator will read as follows:

$$\mathcal{L}\hat{\rho} \Rightarrow \tilde{\mathcal{L}}\vec{\rho} \quad (6)$$

The dephasing super-operators, \mathcal{D}_A and \mathcal{D}_P , are defined by the following equation:

$$\begin{aligned} \tilde{\mathcal{D}}_A &= -\gamma_A \epsilon_c^2(t) (\mathcal{H}_c \mathcal{H}_c \bullet) \\ \tilde{\mathcal{D}}_P &= -\gamma_A (\mathcal{H} \mathcal{H} \bullet) \end{aligned} \quad (7)$$

Where $\tilde{\mathcal{H}}'$ corresponds to the super-operator $-\frac{i}{\hbar}[\hat{\mathbf{H}}', \bullet]$ in Liouville vector space.

More details on vectorization are described in Appendix A.

C. Optimal Control Theory of Open systems (OCT)

Our general task is to mitigate the influence of noise on a quantum gate. We employ quantum optimal control theory (OCT) to provide methods to compute such controls. The

external fields $\{\mathcal{E}_k\}$ interacting with the quantum system have the task of steering the system's dynamics from an initial state to a final state. A more ambitious task is to find the driving field that generates a quantum map $\Lambda(T)$ [29]. The dynamical equation of motion for the map becomes:

$$\frac{d\Lambda(t)}{dt} = \mathcal{L}(t)\Lambda(t) \Rightarrow \frac{d\tilde{\mathcal{G}}}{dt} = \tilde{\mathcal{L}}(t)\tilde{\mathcal{G}}, \quad (8)$$

where $\tilde{\mathcal{G}}$ is the evolution operator in the vector space. The initial condition $\Lambda(t=0) = \mathbb{I}$, where \mathbb{I} is the identity super-operator. The objective is to obtain the optimal driving field $\epsilon(t)$ that induces a given transformation $\hat{\mathcal{O}}$ at $t = T$. This can be interpreted as the mapping of a complete set of operators $\{\hat{\mathbf{A}}\}$ as close as possible to the desired map $\hat{\mathcal{O}}$.

In optimal control theory (OCT), this task is translated to optimizing the objective functional [14]:

$$\mathcal{J}_{max} = \text{Tr}\{\hat{\mathcal{O}}^\dagger\Lambda(T)\} = \sum_j \text{tr}\{(\hat{\mathcal{O}}\hat{\mathbf{A}}_j)^\dagger(\Lambda(T)\hat{\mathbf{A}}_j)\} \Rightarrow \sum_j \text{tr}\{(\tilde{\mathcal{O}}\hat{\mathbf{A}}_j)^\dagger(\tilde{\mathcal{G}}(T)\hat{\mathbf{A}}_j)\} \quad (9)$$

Where $\tilde{\mathcal{G}}$ corresponds to Λ in Hilbert space. We use the symbol Tr for a trace of super-operators, while tr to trace operators in Hilbert space. Two constraints are added to the objective. The first restricts the dynamics to comply with the Liouville-von Neiman equation Eq. (8),

$$\mathcal{J}_{con} = \int_0^T \text{Tr} \left\{ \left(\frac{\partial\Lambda(t)}{\partial t} - \mathcal{L}(t)\Lambda(t) \right) \Upsilon(t) \right\} dt \quad (10)$$

where $\Upsilon(t)$ is a super-operator Lagrange multiplier. The second constraint restricts the total field energy

$$\mathcal{J}_{penal} = \lambda \int_0^T \frac{1}{s(t)} |\epsilon(t)|^2 dt \quad (11)$$

λ is a scalar Lagrange multiplier, and $s(t)$ is a shape function that smoothly turns the pulse on and off. For this task, we choose a Gaussian profile. Adding these constraints, we obtain the overall functional,

$$\mathcal{J}_{Tot} = \left[\text{Tr}\{\hat{\mathcal{O}}^\dagger\Lambda_T\} - \int_0^T \text{Tr} \left\{ \left(\frac{\partial\Lambda(t)}{\partial t} - \hat{\mathcal{L}}(t)\Lambda(t) \right)^\dagger \Upsilon(t) \right\} dt \right] - \lambda \int_0^T \frac{1}{s(t)} |\epsilon(t)|^2 dt, \quad (12)$$

The control task is translated to the maximization of the generalized objective \mathcal{J}_{Tot} , $\delta\bar{\mathcal{J}} = 0$. Functional derivatives with respect to the various functional elements are then taken, Υ, Λ , and ϵ , resulting in the following set of control equations:

1. The Louivile equation Eq. (8) with the initial condition $\Lambda(t=0) = \mathbb{I}$ for Λ .

2. The inverse Louivile equation

$$\frac{\partial \Upsilon(t)}{\partial t} = \mathcal{L}^*(t)\Upsilon(t) \Rightarrow \frac{\partial \tilde{\Upsilon}(t)}{\partial t} = \tilde{\mathcal{L}}^\dagger(t)\tilde{\Upsilon}(t) \quad (13)$$

Where $\tilde{\Upsilon}$ corresponds to Υ in the vector space, with the condition $\Upsilon(t = T) = \hat{\mathcal{O}}^\dagger$. Note that the loss of information in the reverse equation is also inverted so that dephasing occurs from both time ends.

3. The control field update equation for amplitude noise:

$$\Delta \epsilon(t) = -\text{Im} \frac{s(t)[\text{Tr}\{\Upsilon(t)\hat{\mathcal{H}}_c\Lambda(t)\}]}{2(\lambda + \gamma_A[\text{Tr}\{\Upsilon(t)\hat{\mathcal{H}}_c^2\Lambda(t)\})]} \Rightarrow -s(t)\text{Im} \frac{\text{Tr}\{\tilde{\Upsilon}^*\tilde{\mathcal{H}}_c\tilde{\mathcal{G}}(t)\}}{2(\lambda + \gamma_A\text{Tr}\{\tilde{\Upsilon}^*\tilde{\mathcal{H}}_c^2\tilde{\mathcal{G}}(t)\})} \quad (14)$$

$\frac{\partial}{\partial \epsilon}\mathcal{L} = \mathcal{H}_c$ where $\tilde{\mathcal{H}}_c$ is a super operator and corresponds to $\frac{i}{\hbar}[\hat{H}_c, \bullet]$.

The dynamical equations are solved iteratively (counted by k) employing the Krotov method [29, 30], which leads to an update to $\epsilon^{(k)}$:

$$\Delta \epsilon^{(k)}(t) = -\frac{s(t)}{2\lambda} \text{Im} [\text{Tr} \{ \Upsilon^{(k-1)}(t)\mathcal{L}_c\Lambda^{(k)}(t) \}] \Rightarrow -\frac{s(t)}{2\lambda} \text{Im} [\text{Tr} \{ \tilde{\Upsilon}^{(k-1)}(t)\tilde{\mathcal{H}}_c\tilde{\mathcal{G}}^{(k)}(t) \}]. \quad (15)$$

This evaluation continues until certain fidelity ($1 - \mathcal{J}_{max}$) is reached. Note that for most cases $\lambda \gg \gamma_A$, thus one can neglect its term at the denominator.

We solve numerically the dynamics in Eq. (8) and (13) employing a semi-global propagation method [31] described in Appendix B. With these solutions, we update Eq. (15) to update the field and repeat until the desired fidelity is reached. The Krotov method is known to stagger after many iterations. Therefore, we halt this iterative process when stagnation is reached.

III. RESULTS

Optimal control theory is employed first to obtain the desired unitary gate without dissipation. This solution serves as a reference to study the influence of noise on fidelity. At this point, optimal control is used again, including the dissipation to search for control fields that mitigate the impact of noise. The generator of the dynamical map has the form:

$$\tilde{\mathcal{L}} = \tilde{\mathcal{H}}_0 + \tilde{\mathcal{H}}_c + \tilde{\mathcal{D}}_{A/P}. \quad (16)$$

Where $\tilde{\mathcal{D}}$ generates noise where the indices 'A' and 'P' represent the two types of quantum noise defined at Eq. (3) and Eq. (4), respectively.

We choose a driven system that is completely unitary and controllable. This controllability results from commutators of the drift Hamiltonian, $\hat{\mathbf{H}}_0$, and the control Hamiltonian, $\hat{\mathbf{H}}_c$, which generate the full rank algebra [32].

Three representative target gates are studied:

- A Hadamard gate on a single-qubit SU(2)
- A CNOT gate in SU(2) space embedded in SU(4),
- An entangling gate on a 2-qubit system SU(4).

The generator of the dynamical map is Eq. (16), and the cases differ in their Hamiltonians and, as a consequence, their dephasing elements: Eq.'s (3) and (4).

The first step in OCT is to obtain the reference unitary gate, which also establishes a good guess of the control field $\varepsilon(t)$. A good guess can become essential for convergence to high fidelity. In this case, the OC dynamics is generated by:

$$\tilde{\mathcal{L}} = \tilde{\mathcal{H}}_0 + \tilde{\mathcal{H}}_c. \quad (17)$$

We define the fidelity as $F = \text{Tr}\{\hat{\mathcal{O}}^\dagger \Lambda(T)\}$, and infidelity, $IF = 1 - \text{Tr}\{\hat{\mathcal{O}}^\dagger \Lambda(T)\}$. The unitary infidelity is assigned by IF_U .

To test the effect of noise on the infidelity IF_U , we used the solution obtained from IF_U . We propagated a system with noise, Eq. (16) as its generator of the dynamical map.

In figure 1, the degradation of the fidelity by the noise from the infidelity of IF_U to IF_n . We plot the log of ratio $R = \frac{IF_n}{IF_U}$ to the noise rate γ .

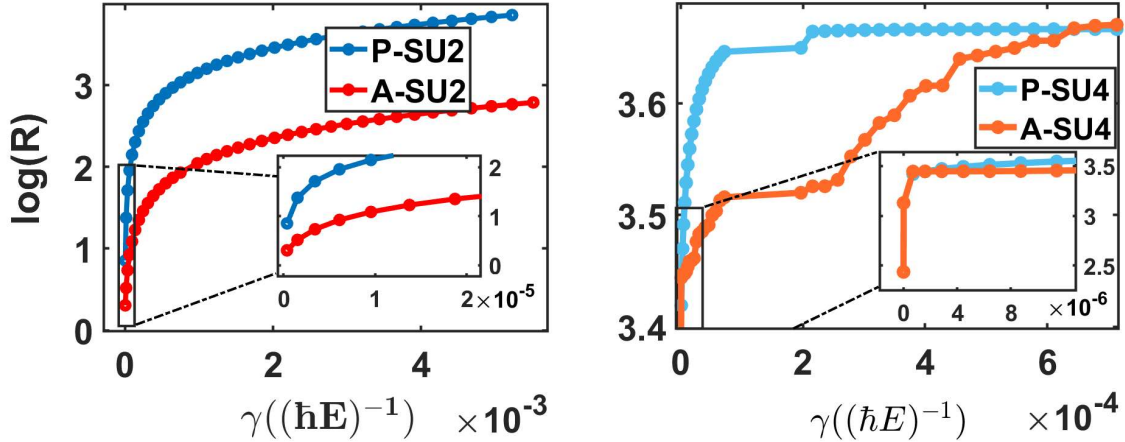


FIG. 1: **Destruction of fidelity by noise.** The change in infidelity of a quantum gate $IF = 1 - \text{Tr}\{\hat{O}^\dagger \Lambda(T)\}$. The reference is a converged unitary control without noise with infidelity IF_U . The same field is used to obtain the gate with noise IF_n . The log of the ratio $R = \frac{IF_n}{IF_U}$, $\log(R) = \log(IF_n) - \log(IF_U)$ is displayed as a function of the noise strength γ . Both phase and amplitude noise are displayed. The insert displays a zoom on the low noise level. Left panel: The single qubit Hadamard gate. Right panel: The two-qubit entangling gate.

Figure 1 shows that amplitude noise \tilde{D}_A is more resilient than the phase noise \tilde{D}_P , for the Hadamard gate. The degradation is significant when the noise strength increases, saturating with three orders of magnitude in infidelity. The two-qubit entangling gate is two orders of magnitude more sensitive than the single-qubit gate with respect to the noise strength γ .

A. Hadamard gate-SU(2) space

The Hadamard gate performs a rotation of π about the axis $(\hat{x} + \hat{z})/\sqrt{2}$ of the Bloch sphere. Expressed as a superoperator in the operator basis $\hat{I}, \hat{S}_X, \hat{S}_Y, \hat{S}_Z$, the Hadamard

gate is given by:

$$\Lambda_U = \begin{pmatrix} 1 & 0 & 0 & 0 \\ 0 & 0 & 0 & -1 \\ 0 & 0 & -1 & 0 \\ 0 & -1 & 0 & 0 \end{pmatrix}. \quad (18)$$

We chose a Hamiltonian, allowing high fidelity for this type of target gate. The drift Hamiltonian:

$$\hat{\mathbf{H}}_0 = u\hat{S}_Z + a_X\hat{S}_X \quad (19)$$

and the control Hamiltonian:

$$\hat{\mathbf{H}}_c = \varepsilon(t)\hat{S}_{XY} \quad (20)$$

where \hat{S}_{XY} is a rotation with an axis in the XY plane (it was found that any direction in this plane leads to control). With this generator, we first obtained the reference unitary gate by OCT, with unitary infidelity $IF_U = 1 \times 10^{-5}$. Using the optimal unitary control field as a guess, solutions under noise are obtained as a function of γ , the noise amplitude. For each value of γ , we apply OCT to mitigate the influence of noise. Figure 2, shows the infidelity improvement as a function of the noise rate, γ for a short control period (2-Rabi cycles $\tau = 4\pi/\Omega$, $\Omega = \sqrt{u^2 + a_X^2}$). The improvement ratio is defined as $NC = \frac{IF_n}{IF_F}$, where IF_n is the infidelity obtained using the unitary guess field subject to noise and IF_F is the infidelity brought by optimal control mitigating the noise.

Figure 3 shows the infidelity improvement for a longer control period (6-Rabi-cycles). When increasing the time allocated for control as shown in Fig. 3, the reference infidelity was maintained to $IF_U \sim 1 \times 10^{-5}$. However, to keep comparable infidelity for both cases, the dephasing rate γ had to be reduced by two orders of magnitude. In both cases, we find that OCT mitigates the influence of noise at low values of γ . When the dissipation increases, the ability to mitigate its influence vanishes.

Infidelity can be mitigated with OC by a factor of two in low noise rates ($<0.2 \times 10^{-3}$) for phase noise and on amplitude noise systems in high noise rate ($\gamma > 0.2 \times 10^{-3}$) systems.

The optimal control formulation restricts the accumulated power Cf. Eq. (11). Nevertheless, we observe that the invested pulse energy in the optimal solution varies with the noise strength γ . The inset of figure 2 shows this dependence. Optimal control must reduce the field strength and, consequently, the controller's noise to battle phase noise at slow noise

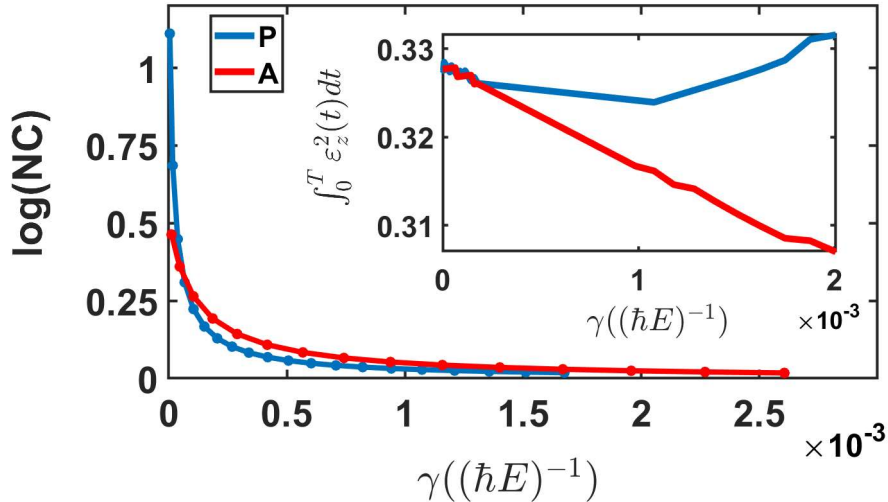


FIG. 2: Noise reduction via Optimal Control for the Hadamard gate for short times (2-Rabi cycles): The noise reduction is defined as $NC = \frac{IF_n}{IF_F}$ Vs the dephasing rate, γ in logarithmic scale. We show here the two dephasing mechanisms, Amplitude noise, \tilde{D}_A , (red, A) and Phase noise, \tilde{D}_P , (blue, P). (inset) The accumulated energy of the control field vs. the dephasing rate in the two dephasing mechanisms.

rates. However, more substantial noise causing significant dephasing can be controlled more effectively only by boosting the field's strength. This is not the case for amplitude noise (\tilde{D}_A); to overcome the noise, OCT reduces the strength of the field and, consequently, the effect of the noise. (Cf. Eq. (24)).

Optimal control mitigation can reduce IF_F for the phase noise more effectively than IF_F of the amplitude noise at low noise rates. This trend is reversed at high rates. The inset of figure 3 shows that the optimal control solution reduces the field's energy for higher dephasing rates, resulting in higher fidelity.

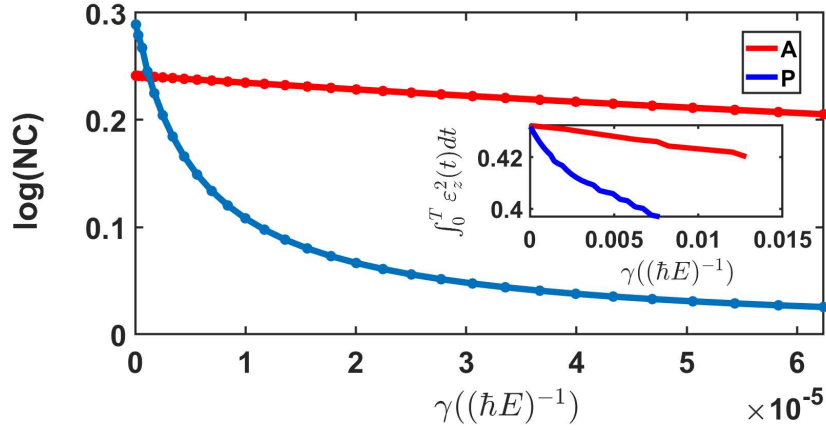


FIG. 3: Noise reduction using Optimal Control for the Hadamard gate at longer times (6-Rabi cycles): The two dephasing mechanisms, amplitude noise, \tilde{D}_A , (red, A) and Phase noise, \tilde{D}_P (blue), (blue, P) are shown. (inset) The accumulated energy of the control field vs. the noise rate in the two noise mechanisms.

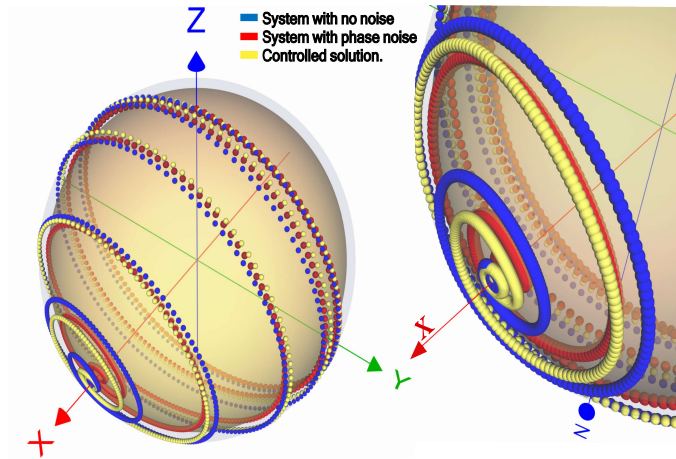


FIG. 4: The trajectory of an initial operator on the Z direction during a Hadamard transformation under phase noise. The reference unitary evolution in blue has an infidelity of $IF_U = 1 \times 10^{-5}$. The trajectory with noise in red does not reside on the surface of the Bloch sphere. The optimal control solution in yellow mitigates the infidelity to a value of $IF_n = 15 \times 10^{-3}$. The right panel zooms on the target state. The outer sphere represents the purity of 1. The inner-sphere purity of 90%.

Figure 4 follows a trajectory of an element of the operator basis during the Hadamard transformation. When the generator is noiseless, the dynamics stay on the surface of the Bloch sphere, and noise pushes the dynamics into the interior of the Bloch sphere. The optimal control mitigation pushes back the trajectory to the surface.

B. CNOT gate - SU(2) embedded in SU(4).

The two-qubit entangling and single-qubit gates comprise a universal computational set that can simulate any quantum circuit. In the subsection, we optimize the control field generating the *CNOT* gate:

$$\hat{U} = \begin{pmatrix} 1 & 0 & 0 & 0 \\ 0 & 1 & 0 & 0 \\ 0 & 0 & 0 & 1 \\ 0 & 0 & 1 & 0 \end{pmatrix} \quad (21)$$

Here, the optimization is carried only for the second qubit, embedded in the two-qubit Hilbert space.

The gate can be realized employing a subspace SU(2) algebra within the SU(4) algebra of the full two-qubit gates. This can be achieved by employing the trivial drift generator:

$$\tilde{\mathcal{H}}_0 = \tilde{\mathcal{I}}^1 \otimes \tilde{\mathcal{I}}^2 \quad (22)$$

and the control generator:

$$\tilde{\mathcal{H}}_c = \varepsilon(t) \sum_{i=X,Y} a_i (\tilde{\mathcal{I}}^1 - \tilde{S}_Z^1) \otimes \tilde{S}_i^2 \quad (23)$$

The two noise models \tilde{D}_A and \tilde{D}_P coincide in this dynamics.

First, we used OCT on the pure unitary dynamics to get IF_U converging to infidelities of $\sim 1 \times 10^{-5}$. Figure 5 shows the fidelity degradation when the noise strength increases.

We now employ this solution as a guess for OCT protocol on noisy systems, partially mitigating noise degradation.

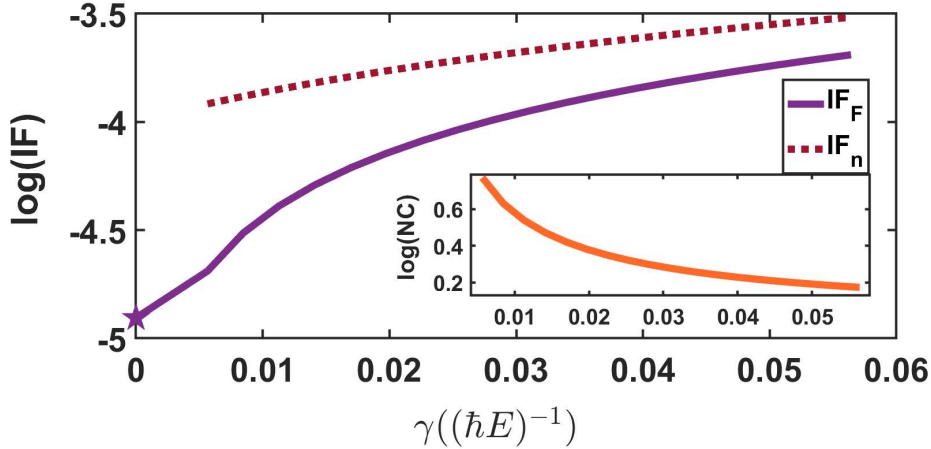


FIG. 5: **Infidelity as a function of the noise strength γ for the C-NOT gate.** The dashed line (brown, IF_n): infidelity employing the unitary control field. The solid line (purple, IF_F): infidelity of the OCT solution mitigating noise. The star represents the infidelity IF_U of the unitary control. (inset) The noise reduction, NC (log scale), Vs. γ .

Figure 5 shows the degradation due to noise IF_n relative to IF_U (star) and the mitigation due to OCT (IF_F). The inset quantifies the noise mitigation due to OCT.

The loss of fidelity of the gate can be caused by a misguided trajectory on the Bloch surface or an unrecoverable loss of purity toward the interior. The instantaneous purity loss

$$\frac{d}{dt}\text{tr}\{\hat{\rho}^2\} = 2\text{tr}\{\hat{\rho}\mathcal{L}\hat{\rho}\} = 2\text{tr}\{\hat{\rho}\mathcal{D}\hat{\rho}\} \quad (24)$$

The second equality is the result that the unitary generator does not change purity. For state-to-state control for pure dephasing, the optimal solution prefers adiabatic following [33] where $\mathcal{D}_P\hat{\rho} = 0$. We must consider the purity loss for all possible inputs for a gate. Thus, the optimal solution is more involved.

Phase noise is equivalent to the noise generated by imperfect timekeeping [26], where the fidelity was found to scales as: $F = (2 + e^{-\frac{\theta^2}{2N}})/3$, where θ is the pulse area and $N \propto 1/\gamma$, is the ticking accuracy. When calculating the fidelity as a function of γ , our results completely agree with this scaling.

For amplitude noise, the instantaneous purity loss becomes in vector notation:

$$\frac{d}{dt}\text{tr}\{\vec{\rho}^2\} = 2 \left(\vec{\rho} \cdot \tilde{\mathcal{D}}_A \vec{\rho} \right) = -\gamma_A \varepsilon_c^2(t) (\vec{\rho} \cdot \mathcal{H}_c \mathcal{H}_c \vec{\rho}) \quad (25)$$

For a pure state, the rate of purity loss for the amplitude noise model becomes [34]:

$$\frac{d}{dt}\text{tr}\{\hat{\rho}^2\} = -2\gamma\varepsilon^2(t)\Delta\hat{\mathbf{H}}_c \quad (26)$$

where $\Delta\hat{\mathbf{H}}_c$ is the variance of the control operator [18]. Examining Eq. (26), the optimal solutions will therefore minimize the control amplitude as the amplitude of noise increases (Cf. Fig. 2 and Fig. 3). For a gate transformation of the term $(\vec{\rho} \cdot \mathcal{H}_c \mathcal{H}_c \vec{\rho})$ in Eq. (25) was found to be almost constant during the propagation, when averaged over a complete set of initial states.

C. Entangling gate-SU(4) space

The ultimate test of optimal control mitigation employs the full pallet of the 16 operator bases of SU(4). The dynamical generators connect all elements of the algebra. Obtaining converged results was difficult. The entangling gate set as a target is:

$$\hat{U} = \begin{pmatrix} 1 & 0 & 0 & 0 \\ 0 & 1 & 0 & 0 \\ 0 & 0 & 0 & i \\ 0 & 0 & -i & 0 \end{pmatrix} \quad (27)$$

Employing many random initial guesses, the maximum fidelity obtained using a single control field was only $\sim 80\%$. We, therefore, modified the drift Hamiltonian such that the two qubits are not in resonance:

$$\tilde{\mathcal{H}}_0 = a\tilde{\mathcal{I}}^1 \otimes \tilde{\mathcal{I}}^2 + \omega_1 \tilde{S}_Z^1 \otimes \tilde{\mathcal{I}}^2 \quad (28)$$

where a is a phase factor and ω_1 is the qubit frequency. In addition, we increased the number of control fields so that the two control generators are:

$${}^Z\tilde{\mathcal{H}}_c = \varepsilon_Z(t) \sum_{i=X,Y} a_i (\tilde{\mathcal{I}} - \tilde{S}_Z)^1 \otimes \tilde{S}_i^2 \quad (29)$$

$${}^E\tilde{\mathcal{H}}_c = \varepsilon_E(t) (\tilde{S}_X^1 \otimes \tilde{S}_Z^2) \quad (30)$$

We tried several random guesses to imitate the control for this model, but none produced high fidelity. We, therefore, employed as a guess field ε_Z obtained from the model of the previous sub-section. The initial guess led to $IF_U \sim 0.05$ on the noiseless system. OC could improve the infidelity to $IF_U \sim 1 \times 10^{-6}$ when the Krotov iterative process reached stagnation.

The CNOT+Phase gate can be part of the universal set. We, therefore, employ it to test the influence of noise.

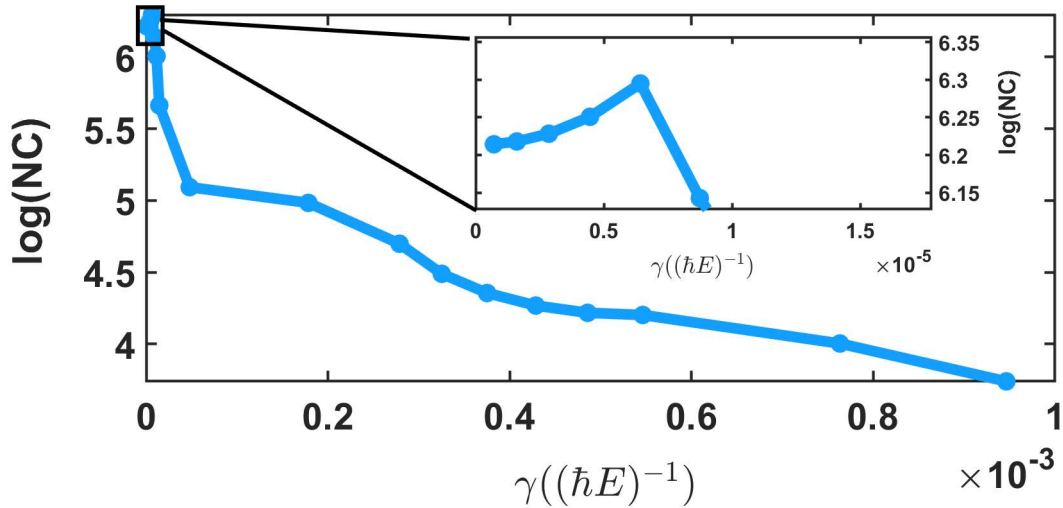


FIG. 6: The noise cancellation $NC = \frac{IF_n}{IF_f}$ (log scale) Vs. the noise rate γ for the entangling gate under phase noise. The insert focuses on the low noise regime.

The infidelity changes due to phase noise for the entangling $SU(4)$ gate are shown in figure 6. The noise significantly degrades the fidelity. Optimal control can recover high fidelity. When the noise rate is low, we overcome the saturation in the Krotov method and obtain infidelities better than the unitary case (Cf. the inset) improving with noise rate. The reason is that Krotov's iterative procedure for systems with noise stagnates much later. New control channels are introduced to the control protocol as suggested in [35]. For higher noise values, the mitigation due to OCT declines as expected.

The influence of amplitude noise on infidelity is shown in Figure 7. Optimal control

managed to restore ~ 4 orders of magnitude. As expected, this mitigation decreases with the growth of the dephasing rate.

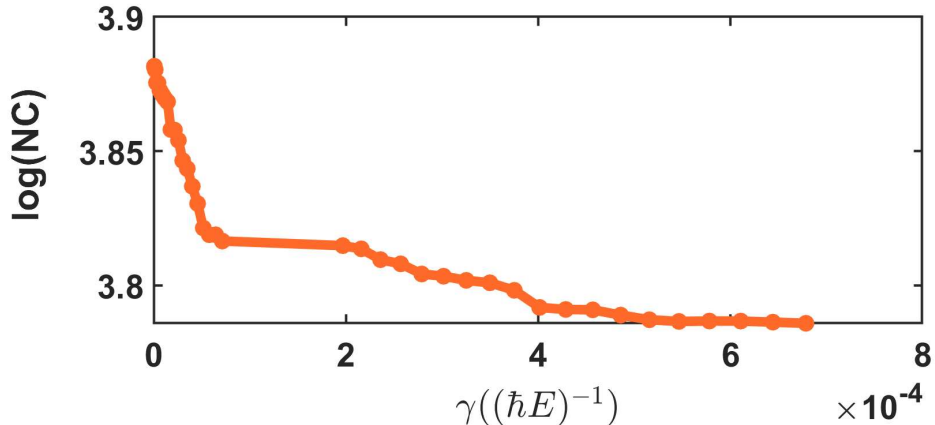


FIG. 7: The noise cancellation $NC = \frac{IF_n}{IF_F}$ (log scale) Vs. the noise rate γ for entangling gate under amplitude noise.

Additional insight was obtained by using the optimal control field with noise to a noiseless propagation. The resulting infidelity was $IF_U \sim 10^{-3}$, 3 orders of magnitude lower than the optimized $IF_U \sim 10^{-6}$. This means that the optimal field with the noise represents a new active solution that emerges due to the control under noise.

IV. CONCLUSIONS

Quantum devices employ interference and entanglement as crucial resources. Dissipation is the primary limiting factor to achieving quantum technology [1, 2]. Significant effort is therefore devoted to isolating the quantum device from the environment. However, the noise originating from the controller is typically ignored. Since such noise is unavoidable, we addressed the question: Can optimal theory achieve the desired quantum gate while mitigating the harm due to noise?

What is unique about controller noise is that it is "hands-off"; the damage is avoided. Our Markovian noise model assumes the controller is fast. A GKLS master equation describes

the quantum dynamics of both amplitude and phase noise. Extension of this study to non-Markovian noise model [24], and Poissonian noise is feasible.

Employing advanced techniques of OCT for open systems, we first find a control that generates a high-fidelity unitary gate. This reference gate studies the degradation of fidelity due to the controller noise. Typically, the system is more sensitive to phase noise. We then apply OCT again to mitigate the fidelity loss due to noise. We have found that quantum control could find control fields that restore fidelity or even surpass it.

The present study could not be possible without a highly accurate propagator addressing explicit time dependence and non-hermitian operators. The gate infidelity we demand is extremely small but significant. The differences between the unitary and noisy solutions are minute.

Our findings emphasize the significance of error mitigation techniques tailored to specific quantum gates and system characteristics. The varying quality of fidelity improvement based on the target gate and system underscores the need for targeted and adaptable strategies in the face of noise.

Notably, the integration of Optimal Control Theory into the framework of open quantum systems led us to discover novel control solutions distinct from noiseless optimal solutions.

In conclusion, our study showcases the potential of Optimal Control Theory in mitigating errors caused by phase and amplitude noise, elevating gate fidelity to new heights within the domain of quantum computing.

ACKNOWLEDGEMENT

We thank Ido Schaefer for his help in implementing the semi-global propagator. In addition we thank Raam Uzdin and Roie Dann for helpful discussions. This study was supported by the Israel Science Foundation (grant nos. 510/17 and 526/21).

Appendix A: Vectorizing Liouville space

The most common and expensive numerical operation in any propagation method is the matrix multiplication of a state vector. The high precision propagators presented in the following appendix contain an even higher order of operations: super-operators acting of

operators. Thus, it is more convenient to vectorize the Liouville space to stay closer to the regular matrix-vector operation. A description of the vectorizing procedure employed in both analytical and numerical aspects. A Hilbert space composed of operators can be generated by defining a scalar product between operators. This is equivalent to a linear space of matrices, converting the matrices effectively into vectors ($\rho \rightarrow |\rho\rangle\rangle$). This is the Fock-Liouville space (FLS) [36]. The usual definition of the scalar product of matrices ϕ and ρ is defined as $\langle\langle\phi | \rho\rangle\rangle \equiv \text{Tr} [\phi^\dagger \rho]$. The Liouville superoperator from Eq. (1) is now an operator acting on the Hilbert space of density matrices. The main utility of the FLS is to allow the matrix representation of the evolution operator. For example, the evolution of a two-level system density matrix can be expressed in the FLS as

$$|\rho\rangle\rangle = \begin{pmatrix} \rho_{00} \\ \rho_{01} \\ \rho_{10} \\ \rho_{11} \end{pmatrix}. \quad (\text{A1})$$

The Liouville von Neumann equation describes the time evolution of a mixed state Eq. (1). In vector notation, the Liouvillian superoperator is expressed as a matrix,

$$\tilde{\mathcal{L}} = \begin{pmatrix} 0 & i\Omega & -i\Omega & 0 \\ i\Omega & iE & 0 & -i\Omega \\ -i\Omega & 0 & -iE & i\Omega \\ 0 & -i\Omega & i\Omega & 0 \end{pmatrix}, \quad (\text{A2})$$

Each row is calculated just by observing the output of the operation $-i[H, \rho]$ in the computational basis of the density matrices space. The system's time evolution corresponds to the matrix equation $\frac{d|\rho\rangle\rangle}{dt} = \tilde{\mathcal{L}}|\rho\rangle\rangle$, which in matrix notation would be

$$\begin{pmatrix} \dot{\rho}_{00} \\ \dot{\rho}_{01} \\ \dot{\rho}_{10} \\ \dot{\rho}_{11} \end{pmatrix} = \begin{pmatrix} 0 & i\Omega & -i\Omega & 0 \\ i\Omega & iE & 0 & -i\Omega \\ -i\Omega & 0 & -iE & i\Omega \\ 0 & -i\Omega & i\Omega & 0 \end{pmatrix} \begin{pmatrix} \rho_{00} \\ \rho_{01} \\ \rho_{10} \\ \rho_{11} \end{pmatrix}. \quad (\text{A3})$$

A similar approach is used for the dissipative part $\tilde{\mathcal{D}}$

Appendix B: Semi-global Propagation method

Obtaining high-fidelity results for controlling quantum gates requires highly accurate and efficient numerical propagators to solve the Liouville von Neumann equation. For this task, we have modified the semi-global propagator [31] to perform in the Liouville vector space.

The Liouville von Neumann equation describes the dynamics of an open quantum system:

$$\frac{d}{dt}\hat{\rho} = \mathcal{L}\hat{\rho} \quad (\text{B1})$$

where $\hat{\rho}$ is the density operator and \mathcal{L} the Liouvillian. For a driven open system, the Liouvillian can be partitioned to:

$$\begin{aligned} \frac{d}{dt}\hat{\rho} = \mathcal{L}_t\hat{\rho} &= (\mathcal{L}_H(t) + \mathcal{L}_D(t))\hat{\rho} \\ \mathcal{L}_H &= \mathcal{L}_{H_0} + \mathcal{L}_{H_t} \end{aligned} \quad (\text{B2})$$

$\mathcal{L}_H(t)$ is the generator of the unitary part of the dynamics and can be decomposed into time-independent and time-dependent components. The dissipative part $\mathcal{L}_D(t)$ implicitly describes the influence of the environment and can be time-dependent.

For a time-independent Lindbladian \mathcal{L}_0 , a formal solution becomes:

$$\hat{\rho}(t) = e^{\mathcal{L}_0 t} \hat{\rho}(0) \quad (\text{B3})$$

with the initial conditions $\hat{\rho}(0)$.

When the Liouvillian can be partitioned into a time-dependent and time-independent part $\mathcal{L} = \mathcal{L}_0 + \mathcal{L}_t$ a formal solution of Eq. (B2) can be written as an integral equation:

$$\hat{\rho}(t) = e^{\mathcal{L}_0 t} \hat{\rho}(0) + \int_0^t e^{\mathcal{L}_0(t-\tau)} \mathcal{L}_t \hat{\rho}(\tau) d\tau \quad (\text{B4})$$

Eq. (B4) will form the basis for the numerical approximation.

In typical control problems \mathcal{L} varies considerably with the time. Therefore, the total evolution is practically broken into finite time steps Δt . Then, one can concatenate the propagators and obtain the total evolution from $t = 0$ to $t = T$ by

$$\vec{\rho}(T) \approx \prod_{j=1}^{N_t} \mathcal{G}_j(\Delta t) \vec{\rho}(0) \quad (\text{B5})$$

where $\mathcal{G}_j(\Delta t)$ is the propagator for t to $t + \Delta t$ where $t = j\Delta t$.

A direct approximation assumes that \mathcal{L}_t is time independent within a time step, then

$$\mathcal{G}_j \approx e^{\mathcal{L}_j \Delta t} \quad (\text{B6})$$

where $\mathcal{L}_j = \mathcal{L}(t + \Delta t/2)$. Sampling \mathcal{L} in the middle of the time step leads to second-order accuracy in Δt .

In what follows, we formulate the density operator as a vector $\vec{\rho}$ and the Liouvillian superoperator \mathcal{L} as a matrix (see above App. A [28]).

A numerical method to solve Eq.(B6) is based on expanding the exponent or any analytic function in a polynomial series in the matrix \mathcal{L}_j :

$$\vec{\rho}(t + \Delta t) \approx \sum_{n=0}^{K-1} a_n(t + \Delta t) P_n(\mathcal{L}_j) \vec{\rho}(t) \quad (\text{B7})$$

where $P_n(\mathcal{L}_j)$ is a polynomial of degree n , and $a_n(t + \Delta t)$ is the corresponding expansion coefficient in the interval $t, t + \Delta t$. This requires choosing the set of expansion polynomials $P_n(\mathcal{L}_j)$ and the corresponding coefficients a_n [37].

The expansion (B7) has to be accurate in the eigenvalue domain of \mathcal{L}_j so that the form (B7) will be helpful to represent \mathcal{G}_j . Successive matrix-vector multiplications can compute this series of polynomials at Eq. (B7). It scales as $O(N^2)$, and the computational effort can be reduced even further. For sparse superoperators, the matrix-vector operation can be replaced by an equivalent semi-linear scaling, with $\sim O(N)$ [38].

An immediate question is how to choose the set of expansion polynomials $P_n(x)$. As a thumb rule, we search for a polynomial basis that converges the fastest. An orthogonal set of polynomials is the first step for fast convergence [39].

An efficient implementation can be done recursively. The Chebyshev polynomial and Newton interpolation polynomials are two orthogonal expansion series using $P_n(\mathcal{L}_j)$. When the Hamiltonian is non-Hermitian, the eigenvalue domain becomes complex, and the Chebyshev approach is not appropriate anymore. Then, the Newtonian or Arnoldi approach should be used instead [39–41].

Note that in Eq. (B3), only the coefficients $a_n(t)$ are time-dependent. The solution at intermediate time points can be obtained by calculating the coefficients for intermediate points with negligible additional computational effort.

Quantum control of gates requires exceptionally high accuracy. The convergence rate of Eq. (B5) with a piecewise constant \mathcal{L}_j is slow, leading to extensive numerical effort. To

obtain faster convergence, we must consider the problem of time ordering within the time step Δt .

To overcome the problem of time ordering, we will combine the polynomial solution of Eq. (B3) and the integral equation formal solution (B4). In Eq. (B4), the free propagator appears both as a free term and at the integrand. The solution of the integral equation requires an iterative approach since $\hat{\rho}(\tau)$ appears also in the integrand. The iteration is carried out by extrapolating the solution from one time step to the next, t to $t + dt$.

The integral in the formal solution Eq. (B4) is reformulated as an inhomogeneous source term:

$$\frac{d\vec{\rho}(t)}{dt} = \mathcal{L}_j \vec{\rho}(t) + \vec{\mathfrak{s}}(t) \quad (\text{B8})$$

The source term will represent the time-dependent/nonlinear part of the dynamics.

Treating Eq. (B8) as an inhomogeneous ODE will give rise to a formal solution to the time-dependent problem. We can write the solution to Eq. (B3):

$$\begin{aligned} \vec{\rho}(t + \Delta t) &= \tilde{\mathcal{G}}_j(t) \vec{\rho}(t) + \int_t^{t+\Delta t} \tilde{\mathcal{G}}_j(t - \tau) \vec{\mathfrak{s}}(\tau) d\tau \\ &= \exp(\mathcal{L}_j t) \vec{\rho} + \int_t^{t+\Delta t} \exp[\mathcal{L}_j(t - \tau)] \vec{\mathfrak{s}}(\tau) d\tau \\ &= \exp(\mathcal{L}_j t) \vec{\rho}_0 + \exp(\mathcal{L}_j t) \int_t^{t+\Delta t} \exp(-\mathcal{L}_j \tau) \vec{\mathfrak{s}}(\tau) d\tau \end{aligned} \quad (\text{B9})$$

Where $\tilde{\mathcal{G}}_j$ is defined as the time-independent propagator by the vec-ing procedure: subsection II B.

The source term is expanded as a time-dependent polynomial to solve for the integral analytically.

$$\vec{\mathfrak{s}}(t) = \sum_{n=0}^{M-1} \frac{t^n}{n!} \vec{\mathfrak{s}}_n \quad (\text{B10})$$

This expansion allows us to solve formally the integral in Eq. (B9)

$$\int e^{at} t^m / m! = \sum_{n=1}^m e^{at} t^{n-m} / a^n (n-m)!.$$

The problem is now shifted to obtaining the expansion coefficients $\vec{\mathfrak{s}}_m$. This task is obtained by approximating $\vec{\mathfrak{s}}(t)$ by an orthogonal polynomial in the time interval. We chose a Chebyshev expansion

$$\vec{\mathfrak{s}}(t) \approx \sum_{n=0}^{M-1} \vec{\mathfrak{b}}_n T_n(t) \quad (\text{B11})$$

where the coefficients $\vec{\mathbf{b}}_n$ are computed by a scalar product of the $T_n(t)$ with $\vec{\mathbf{s}}(t)$. Approximating the coefficients using Chebychev sampling points in the time interval Δt .

The coefficients $\vec{\mathbf{s}}_m$ are calculated by relating the polynomial Eq. (B11) to the Chebychev expansion. This source term is inserted into the integral Eq. (B9), leading to a numerical approximation to the solution of the TDLE. The addition of the source term into the dynamics gives rise to an analytical solution for the last term in Eq. (B9), presented here on the RHS of Eq. (B12)

$$J_{m+1}(\mathcal{L}_j, t) \equiv \int_t^{t+\Delta t} \exp(-\mathcal{L}_j \tau) \tau^m d\tau, \quad m = 0, 1, \dots \quad (\text{B12})$$

with the recursion relations:

$$J_m(\mathcal{L}_j, t) = -\frac{\exp(-\mathcal{L}_j t) t^{m-1}}{\mathcal{L}_j} + \frac{m-1}{\mathcal{L}_j} J_{m-1}(\mathcal{L}_j, t), \quad m = 2, 3, \dots \quad (\text{B13})$$

where

$$J_1(\mathcal{L}_j, t) \equiv \int_t^{t+\Delta t} \exp(-\mathcal{L}_j \tau) d\tau = \frac{1 - \exp(-\mathcal{L}_j t)}{\mathcal{L}_j}.$$

Plugging Eq. (B10) into this formulation leads to the following:

$$\exp(\mathcal{L}_j, t) \sum_{n=0}^{M-1} \frac{1}{n!} \int_0^t \exp(-\mathcal{L}_j \tau) t^n d\tau s_n = \exp(\mathcal{L}_j t) \sum_{n=0}^{M-1} \frac{1}{n!} J_{n+1}(\mathcal{L}_j, t) s_n = \sum_{n=0}^{M-1} f_{n+1}(\mathcal{L}_j, t) s_n \quad (\text{B14})$$

In Eq. (B2), the Louivilian was split into explicit time-dependent and approximated time-independent parts; this partition is used to re-write the TDLE

$$\frac{d\vec{\rho}(t)}{dt} = \mathcal{L}_j \vec{\rho}(t) + \vec{\mathbf{s}}(\vec{\rho}(t), t) \quad (\text{B15})$$

Which is a reformulation of Eq. (B8). The same analysis leads to:

$$\vec{\rho}(t, t + \Delta t) = \exp(\mathcal{L}_j t) \vec{\rho}(t) + \exp(\mathcal{L}_j t) \int_t^{t+\Delta t} \exp(-\mathcal{L}_j \tau) \vec{\mathbf{s}}(\vec{\rho}(\tau), \tau) d\tau \quad (\text{B16})$$

Now, we can use these formulations to approximate Eq. (B16):

$$\vec{\rho}(t, t + \Delta t) \approx P_M(\mathcal{L}_j, (t, t + \Delta t)) \vec{S}(t, t + \Delta t)_M + \sum_{n=0}^{M-1} \frac{t^n}{n!} \vec{S}(t, t + \Delta t)_n \quad (\text{B17})$$

$P_M(\mathcal{L}_j, (t, t + \Delta t)) \vec{S}(t, t + \Delta t)_M$, is approximated by the Arnoldi method (the eigenvalue spectrum of \mathcal{L} is distributed on the complex plane) where

$$\vec{S}(t)_M \equiv \vec{\mathbf{s}}(t) + \mathcal{L}_t \vec{\rho}(t)$$

are computed by expanding it by time in the same form of (B10). We have used here the fact that $P_n(\mathcal{L}_{\mathcal{H}}, t) = \mathcal{L}_{\mathcal{H}}^{k-n} P_k(\mathcal{L}_{\mathcal{H}}, t) + \sum_{j=n}^{k-1} \frac{t^j}{j!} \mathcal{L}_{\mathcal{H}}^{j-n}$ Eq. (B17) and \vec{s}_j includes dependence on $\vec{\rho}(t)$. It would seem we are back to the same problem. Nevertheless, it can be overcome by an iterative procedure. First, we guess a solution $\vec{\rho}_g(t)$, within a time step Δt and use it in Eq. (B17) to obtain a new approximate solution. This procedure can be continued until the solution converges with the desired accuracy. The initial guess is extrapolated from the previous time step to accelerate convergence.

Three numerical parameters determine the precision of the propagation and the convergence rate:

- The size of the time step Δt .
- Number of Chebyshev sampling points in each time step M .
- The size of the Krylov space K corresponds to the basis of the Arnoldi algorithm. It is important to note that this parameter is limited by $Dim\{\mathcal{L}\} - 1$

Each of those is adjustable by the user to fit their needs best. For example, in the Hadamard transformation system, we have used the following parameters: $\Delta t = 0.1, M = 7$, and $K = 3$. With these parameters, we got an accuracy of 10^{-8} for the propagator, two orders of magnitude higher than the fidelity of the target transformation. For the entangling gate, we adjusted the parameters for a higher resolution that would fit 10^{-8} for the fidelity of the target transformation ($M = K = 9$).

-
- [1] J. Preskill, Quantum **2**, 79 (2018).
- [2] M. Schlosshauer, Physics Reports **831**, 1 (2019).
- [3] K. Kraus, Annals of Physics **64**, 311 (1971).
- [4] V. Gorini and A. Kossakowski, Journal of Mathematical Physics **17**, 1298 (1976).
- [5] G. Lindblad, Communications in Mathematical Physics **48**, 119 (1976).
- [6] A. Bartana, R. Kosloff, and D. J. Tannor, The Journal of chemical physics **106**, 1435 (1997).
- [7] Y. Ohtsuki, W. Zhu, and H. Rabitz, The Journal of chemical physics **110**, 9825 (1999).
- [8] A. Bartana, R. Kosloff, and D. J. Tannor, Chemical Physics **267**, 195 (2001).

- [9] T. Schulte-Herbrüggen, A. Spörl, N. Khaneja, and S. Glaser, *Journal of Physics B: Atomic, Molecular and Optical Physics* **44**, 154013 (2011).
- [10] C. P. Koch, *Journal of Physics: Condensed Matter* **28**, 213001 (2016).
- [11] B. Pokharel, N. Anand, B. Fortman, and D. A. Lidar, *Physical review letters* **121**, 220502 (2018).
- [12] V. Petruhanov and A. Pechen, *Journal of Physics A: Mathematical and Theoretical* **56**, 305303 (2023).
- [13] G. J. Delben, M. W. Beims, and M. G. E. da Luz, *Phys. Rev. A* **108**, 012620 (2023).
- [14] V. Petruhanov and A. Pechen, arXiv preprint arXiv:2309.02063 (2023).
- [15] R. Dann and R. Kosloff, *Quantum* **5**, 590 (2021).
- [16] S. Kallush, R. Dann, and R. Kosloff, *Science Advances* **8**, eadd0828 (2022).
- [17] L. Viola, E. Knill, and S. Lloyd, *Physical Review Letters* **82**, 2417 (1999).
- [18] M. Khasin and R. Kosloff, *Physical review letters* **106**, 123002 (2011).
- [19] S. Kallush, M. Khasin, and R. Kosloff, *New Journal of Physics* **16**, 015008 (2014).
- [20] X. Jiang, J. Scott, M. Friesen, and M. Saffman, *Physical Review A* **107**, 042611 (2023).
- [21] H.-P. Breuer, F. Petruccione, *et al.*, *The theory of open quantum systems* (Oxford University Press on Demand, 2002).
- [22] V. Gorini, A. Kossakowski, and E. C. G. Sudarshan, *Journal of Mathematical Physics* **17**, 821 (1976).
- [23] T. Feldmann and R. Kosloff, *Europhysics Letters* **89**, 20004 (2010).
- [24] A. Kiely, *Europhysics Letters* **134**, 10001 (2021).
- [25] R. Kosloff and T. Feldmann, *Physical Review E* **82**, 011134 (2010).
- [26] J. Xuereb, P. Erker, F. Meier, M. T. Mitchison, and M. Huber, arXiv preprint arXiv:2301.10767 (2023).
- [27] G. S. Agarwal, *Phys. Rev. Lett.* **37**, 1383 (1976).
- [28] M. Am-Shallem, A. Levy, I. Schaefer, and R. Kosloff, arXiv preprint arXiv:1510.08634 (2015).
- [29] J. P. Palao and R. Kosloff, *Physical Review A* **68**, 062308 (2003).
- [30] V. Krotov, *Global methods in optimal control theory*, Vol. 195 (CRC Press, 1995).
- [31] I. Schaefer, H. Tal-Ezer, and R. Kosloff, *Journal of Computational Physics* **343**, 368 (2017).
- [32] V. Ramakrishna and H. Rabitz, *Physical Review A* **54**, 1715 (1996).
- [33] A. Levy, A. Kiely, J. G. Muga, R. Kosloff, and E. Torrontegui, *New Journal of Physics* **20**,

- 025006 (2018).
- [34] S. Boixo, L. Viola, and G. Ortiz, *Europhysics Letters* **79**, 40003 (2007).
 - [35] R. Wu, A. Pechen, C. Brif, and H. Rabitz, *Journal of Physics A: Mathematical and Theoretical* **40**, 5681 (2007).
 - [36] D. Manzano, *Aip Advances* **10** (2020).
 - [37] M. Berman and R. Kosloff, *Computer physics communications* **63**, 1 (1991).
 - [38] D. Kosloff and R. Kosloff, *Journal of Computational Physics* **52**, 35 (1983).
 - [39] R. Kosloff, *Annual review of physical chemistry* **45**, 145 (1994).
 - [40] W. E. Arnoldi, *Quarterly of applied mathematics* **9**, 17 (1951).
 - [41] R. B. Lehoucq and D. C. Sorensen, *SIAM Journal on Matrix Analysis and Applications* **17**, 789 (1996).